Supplementary information

AGE MODEL

The duration of the time lag (t_{lag}) depends crucially on the local sedimentation rate. Marine and terrestrial sections through the PETM can be divided into three phases defined by the vertical expression of the $\delta^{13}C$ curve (Bowen et al., 2006): onset, body and recovery phases. The durations of each of these phases (Table DR1) are used along with the measured stratigraphic thickness to determine a time-averaged sedimentation rate for each section in northern Spain (Table DR2) and central USA (Tables DR3 and DR4). Sedimentation rate can vary be a function of measurement window (e.g. stratigraphic thickness), however the similarity of sedimentation rates calculated for different phases for the central USA sites suggest that linear extrapolation of the age model is robust.

SEDIMENT TRANSPORT MODEL

We model sediment transport using the methods described in Armitage et al., (2016), which we describe briefly below. The 1D numerical model solves for the change in topography due to the transport of sediment down slope. In the terrestrial domain, sediment flux is a function of both local slope and surface water flux following Smith and Bretherton (1972):

$$q_s = -(\kappa + c q_w)\, dz/dx$$

where z is elevation, x is the down system distance, κ is the linear diffusion coefficient, c is the fluvial transport coefficient, $n \geq 1$, and the water flux is given by:

$$q_w = \alpha x$$

where α is the precipitation rate. At the input boundary we introduce a sediment flux and a water flux given by the precipitation rate multiplied by the assumed catchment length which we assume is 100 km long. Terrestrial sediment transport is assumed to extend from the left hand input boundary until the topography is below sea level. At this point we assume that the mechanism for sediment transport change from surface run-off to sediment transport as a function of tidal and wave energy. Following Kaufman et al. (1991) we take a simple heuristic law for sediment transport as a function of water depth,

$$q_s = -\kappa_{sea}\, exp(-\kappa_{decay}(z_{sea} - z))\, dz/dx$$

where κ_{sea} sea is the linear diffusion coefficient for subaqueous sediment transport and κ_{decay} is the coefficient that parameterizes the effect of water depth (Z_{sea}) on subaqueous sediment transport. The change in elevation with time is then given from the Exner equation of mass conservation:

$$dz/dt = U - dq_s/dx,$$

where U is the subsidence (negative uplift) and takes the form of a exponential that decreases in magnitude away from the left hand boundary (Fig. DR1). The values chosen for the various coefficients and parameters are listed in Table DR5.

Grain size fining is calculated from the area of sediment deposited in each numerical time step. Grain size sorting follows the methods described in Armitage et al. (2015), which uses the sorting model of Fedele and Paola (2007) for grain sizes larger than 2 mm, and for grain sizes smaller than 2 mm a simple Sternberg-type exponential sorting model is assumed (Sternberg, 1875; Robinson and Slingerland, 1998); the work here focuses on grain sizes larger than 2 mm in the terrestrial segment. The system of equations is solved using a finite element numerical model as described in Armitage et al. (2016) for a total duration of 15 Myr, where a perturbation to the precipitation rate is introduced after 10 Myr. The model domain is 2000 km long. The assumed input sediment flux is 40 m^2yr^{-1} with a gravel fraction of 5% and mean grain size of 50 mm and standard deviation of 100 mm. Precipitation rate is varied following a box profile whereby the magnitude of change in precipitation rate is increased from 0.5 $mmyr^{-1}$ to 0.75 $mmyr^{-1}$, 1 $mmyr^{-1}$, 1.25 $mmyr^{-1}$ and 1.5 $mmyr^{-1}$.over a fixed duration of 5 kyrs. The resulting stratigraphic section from the model shows that the increase in precipitation rate leads to erosion of the topmost deposits and the progradation of a conglomeratic sheet down system (Figure DR1). There is then a break in slope at the coastline where the mechanisms of sediment transport changes.

The linear diffusion coefficient (κ) and the fluvial diffusion transport coefficient (c) are independent of input grain size in our model set-up. And so changing the input grain size distribution on the input sediment supply has no impact on the duration of the time lag. However varying the input grain size will have the effect of increasing (finer GSD) or decreasing (coarser GSD) the fluvial transport coefficient (e.g. Paola et al., 1992), which will of course affect response and stratigraphic lag duration. The larger the value of the fluvial transport coefficient, the shorter the duration of the stratigraphic lag (see Armitage et al.,

2013). In addition, response time and stratigraphic lag duration will scales with system length; an increase in the length of the transport system will cause an increase in the response time and duration of stratigraphic lag.

The code is available here: https://bitbucket.org/johnjarmitage/sealand-petm.

SUPPLEMENTARY TABLES

Onset (kyrs)	Body (kyrs)	Recovery (kyrs)	Onset, Body+Recovery (kyrs)	Reference
	–	–	150-200	Kennet and Stott (1991)
	–	–	150	Norris and Rohl (1999)
35	45	50	130	Bowen et al., (2004)
>4	–	–	–	Zeebe et al (2016)
20	–	–	–	Cui et al (2011)
10-20	113	83	216	Murphy et al. (2010)
8-23	–	–	–	McInerney & Wing (2011) - terrestrial
	–	–	170	Rohl et al (2000)

Table DR1: Duration of the carbon isotope excursion for PETM and phases within

Section	Excursion thickness (mm)	Lag thickness (mm)	Accumulation rate (mm yr^{-1})	Time lag (yr)
Tendrui	45000	6000	0.45†	22857
Tendrui	45000	6000	0.25¥	35556
Campo	6000	2000	0.1†	25000
Campo	6000	2000	0.06¥	36364
Claret	38000	5000	0.38†	17241
Claret	38000	5000	0.21¥	26316
Esplugafreda	0	0	0.1	0

Table DR2: Time lag calculation of the Spain sections. †Sedimentation rate calculated assuming linear sedimentation rates across the excursion thickness assuming 100 kyr-long isotope excursion. ¥ Sedimentation rate calculated assuming linear sedimentation rates across the excursion thickness assuming 180 kyr-long isotope excursion.

Excursion thickness (mm)	Lag thickness (mm)	Accumulation rate (mm yr^{-1})	Time lag (yr)
40000	9000	0.36[1]	27500
40000	9000	0.22[2]	40500
40000	9000	0.4[3]	22500

Table DR3. Time lag calculation of the DeBeque section, Colorado (Foreman et al., 2012) [1]accumulation rate quoted. [2]Sedimentation rate calculated assuming linear sedimentation rates across the excursion thickness assuming 180 kyr-long isotope excursion. [3]Sedimentation rate calculated assuming linear sedimentation rates across the excursion thickness assuming 100 kyr-long isotope excursion.

Excursion thickness (mm)	**Lag thickness (mm)**	**Accumulation rate (mm yr^{-1})**	**Time lag (yr)**
55000	7000	0.28[1]	25200
55000	7000	0.5[2]	14000
55000	7000	0.35[5]	22857

Table DR4. Time lag calculation of Bighorn basin section, Wyoming (Foreman 2014) [1]Sedimentation rate calculated using excursion thickness and 180 kyr-long isotope excursion. [2]Sedimentation rate calculated using excursion thickness and 100 kyr-long isotope excursion. [3]Long-term sediment accumulation rate using magnetostratigraphy.

Parameter	**Description**	**Value**
κ	Linear hill slope diffusion coefficient	1 m^2yr^{-1}
c	Fluvial transport coefficient	0.1
n	Transport exponent	1
κ_{sea}	Subaqueous diffusion coefficient	$5x10^4$ m^2yr^{-1}
κ_{decay}	Subaqueous diffusion decay coefficient	$2x10^4$ m^{-1}

Table DR5. Model parameter description and values

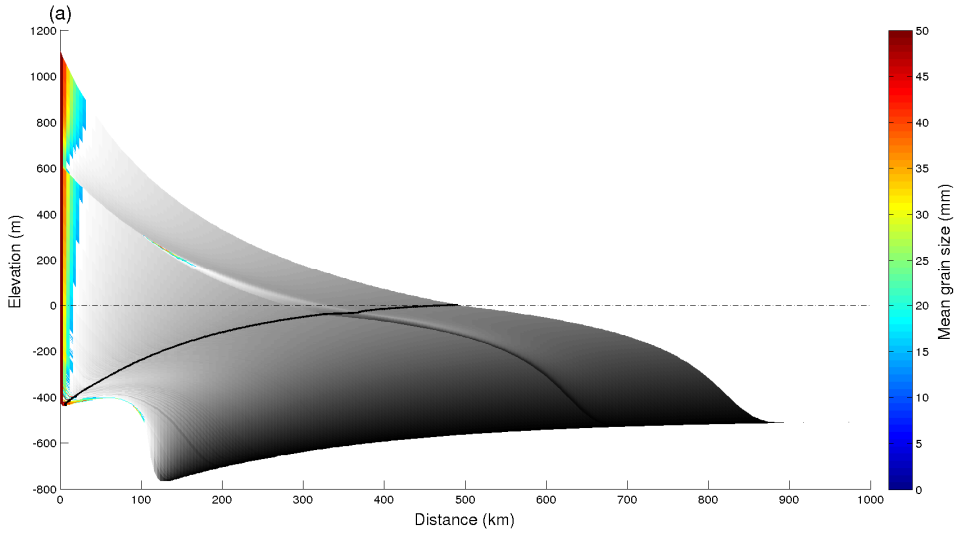

Figure DR1: Model stratigraphy for the full model duration of 15 Myr. The perturbation to the precipitation rate occurs at a model time of 10 Myr. Colours show the predicted grain size distribution for grains larger than 2 mm. The grey scale shows the distribution of grains less than 2 mm in size. The solid dark line is the shoreline trajectory and the dashed line is the model sea level. The model domain extends to 2000 km in the x-direction.

REFERENCES CITED

Armitage, J.J., Allen, P.A., Burgess, P.M., Hampson, G.J., Whittaker, A.C., Duller, R.A, and Michael, N.A., 2015, Physical stratigraphic model for the Eocene Escanilla sediment routing system: Implications for the uniqueness of sequence stratigraphic architectures: Journal of Sedimentary Research, v. 85, p. 1510-1524.

Armitage, J.J., Burgess, P.M., Hampson, G.J., and Allen, P.A., 2016, Deciphering the origin of cyclical gravel front and shoreline progradation and retrogradation in the stratigraphic record: Basin Research, v. 30, p. 15-35, doi:10.1111/bre.12203.

Bowen, G.J., Beerling, D.J., Koch, P.L., Zachos, J.C., and Quattlebaum, T., 2004, A humid climate state during the Palaeocene-Eocene thermal maximum: Nature, v. 432, p. 495–499, doi:10.1038/nature03115.

Bowen, G.J., Bralower, T.J., Delaney, M.L., Dickens, G.R., Kelly, D.C., Koch, P.L., Kump, L.R., Meng, J., Sloan, L.C., Thomas, E., Wing, S.L., and Zachos, J.C., 2006, Eocene hyperthermal event offers insight into greenhouse warming: Eos (Transactions, American Geophysical Union), v. 87, p. 165-169.

Cui, Y., Kump, L.R., Ridgwell, A.J., Charles, A.J., Junium, C.K., Diefendorf, A.F., Freeman, K.H., Urban, N.M., and Harding, I.C., 2011, Slow release of fossil carbon during the Palaeocene-Eocene Thermal Maximum: Nature Geoscience, v. 4, p. 481-485.

Fedele, J., and Paola, C., 2007, Similarity solutions for fluvial sediment fining by selective deposition: Journal of Geophysical Research - Earth Surface, v. 112, F02038, doi: 10.1029/2005JF000409.

Foreman, B.Z., Heller, P.L., and Clementz, M.T., 2012, Fluvial response to abrupt global warming at the Paleocene/Eocene boundary: Nature, v. 491, p. 92-95.

Foreman, B.Z., 2014, Climate-driven generation of a fluvial sheet sand body at the Paleocene-Eocene boundary in north-west Wyoming (USA): Basin Research, v. 26, p. 25-241.

Kaufman, P., Crotzinger, J.P., and McCormick, D.S., 1991, Depth-dependent diffusion algorithm for simulation of sedimentation in shallow marine depositional systems: Bulletin of the Kansas Geological Survey, v. 233, 489-508.

Kennett, J.P., and Stott, L.D., 1991, Abrupt deep-sea warming, palaeoceanographic changes and benthic extinctions at the end of the Palaeocene: Nature, v. 353, p. 225-229.

McInerney, F.A., and Wing, S.L., 2011, The Paleocene-Eocene Thermal Maximum: A Perturbation of Carbon Cycle, Climate, and Biosphere with Implications for the Future: Annual Review of Earth and Planetary Sciences, v. 39, p. 489-516.

Murphy, B.H., Farley, K.A., and Zachos, J.C., 2010, An extraterrestrial 3He-based timescale for the Paleocene–Eocene thermal maximum (PETM) from Walvis Ridge, IODP Site 1266: Geochimica et Cosmochimica Acta, v. 74, p. 5098-5108.

Norris, R.D., and Röhl, U., 1999, Carbon cycling and chronology of climate warming during the Palaeocene/Eocene transition: Nature, v. 401, p. 775-778.

Paola, C., Heller, P. and Angevine, C. (1992), The large-scale dynamics of grain size variation in alluvial basins: 1. Theory: Basin Research, v.4, p. 73-90.

Röhl, U., Westerhold, T., Strasse, L., Bralower, T.J., Zachos, J.C., 2007, On the duration of the Paleocene-Eocene thermal maximum (PETM): Geochemistry, Geophysics, Geosystems, v. 8, Q12002, doi:10.1029/2007GC001784.

Robinson, R.A.J., and Slingerland, R.L., 1998, Origin of fluvial grain-size trends in a foreland basin the: Pocono Formation on the Central Appalachian Basin: Journal of Sedimentary Research, v. 68, p. 473-486.

Smith, T.R. and Bretherton, F.P., 1972, Stability and conservation of mass in drainage basin evolution: Water Resources Research, v. 8, p. 1506–1529.

Sternberg, H., 1875, Untersuchungen über Längen und Querprofil geschiebeführnde Flüsse: Zeitschrift fur das Bauwesen, v. 25, p. 483-506.

Zeebe, R.E., Ridgwell, A., and Zachos, J.C., 2016, Anthropogenic carbon release rate unprecedented during the past 66 million years: Nature Geoscience, v. 9, p. 325-329.